Dalton Transactions

Accepted Manuscript

ROYAL SOCIETY OF CHEMISTRY

www.rsc.org/dalton

Synthesis, Crystal Structure, and Transport Properties of $Cu_{2.2}Zn_{0.8}SnSe_{4-x}Te_x$ ($0.1 \leq x \leq 0.4$)

Yongkwan Dong [a], Brian Eckert [a], Hsin Wang [b], Xiaoyu Zeng [c], Terry M. Tritt [c], George S. Nolas [a,*]

[a] *Department of Physics, University of South Florida, Tampa, FL 33620, USA*

[b] *Materials Science and Technology Division, Oak Ridge National Laboratory, Oak Ridge, TN 37831, USA*

[c] *Department of Physics and Astronomy, Kinard Laboratory, Clemson University, Clemson, SC 29634, USA*

* E-mail: gnolas@usf.edu

Table of Contents Entry

The synthesis, crystal structure and transport properties of $Cu_{2.x}Zn_{0.8}SnSe_{4-x}Te_x$ (x = 0.1~0.4) series were investigated. $Cu_{2.2}Zn_{0.8}SnSe_{3.7}Te_{0.3}$ has a *ZT* value of 0.56 at 700 K, the highest *ZT* value thus far reported for solid-solution compositions in this material system.

Table of Contents Artwork

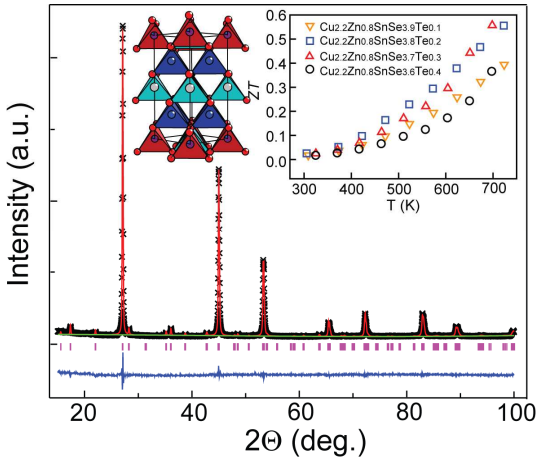

ABSTRACT

Quaternary chalcogenides, particular compounds with the stannite structure-type, are of interest for thermoelectrics applications however tellurium-containing compositions have not been extensively investigated. We report on the synthesis and high temperature thermoelectric properties of *p*-type stannites $Cu_{2.2}Zn_{0.8}SnSe_{4-x}Te_x$ (x = 0.1, 0.2, 0.3, and 0.4). The compositions for each specimen were confirmed with a combination of Rietveld refinement and elemental analysis. Hall measurements indicate that holes are the dominant charge carriers in these materials. The electrical resistivity shows little temperature dependence up to 500 K and then increases with increasing temperature. The thermal conductivity decreases with increasing temperature with no indication of increase at higher temperatures suggesting a minimal bipolar diffusion effect in the thermal conductivity although these materials possess relatively small band-gaps as compared to that of other stannite compositions. A maximum *ZT* value of 0.56 was obtained at 700 K for $Cu_{2.2}Zn_{0.8}SnSe_{3.7}Te_{0.3}$ due to a relatively high Seebeck coefficient and low thermal conductivity.

INTRODUCTION

Thermoelectric devices are of interest for waste heat recovery and solid-state cooling applications.[1] A good thermoelectric material has a large dimensionless figure-of-merit, ZT (= $S^2T/\rho\kappa$, where S is the Seebeck coefficient, ρ the electrical resistivity, κ the thermal conductivity, and T is the absolute temperature) in the temperature range of interest. Typically ZT can be optimized by doping; however, these three parameters are not independent of each other.[1-4] Recent research on the thermoelectric properties of existing or new materials, and their synthesis and subsequent optimization, have focused on an understanding of their structure–property relationships.

Quaternary chalcogenides, particularly the stannite structure-type such as $Cu_2ZnSnSe_4$ and $Cu_2CdSnSe_4$, have recently been investigated as potential candidates for thermoelectric power generation applications due to their intrinsically low κ that is strongly influenced by their structural features.[5,6] Although these materials possess relatively wide band gaps, a property that is typically not of interest for thermoelectric applications,[4] the electrical properties can be modified by appropriate doping and/or variations in stoichiometry. Investigating nano-scale effects on the thermoelectric properties have also been reported.[7-9] Further reduction of κ is achievable by alloying whereby point defect scattering induced by local anisotropic structural disorder leads to a reduction in the lattice thermal conductivity, κ_L.[10-17] Consequently certain stannite compositions have been shown to exhibit relatively good ZT values. Nevertheless the ρ values are relatively high as compared with that of state-of-the-art thermoelectric materials.[3] Herein we report on the synthesis, crystal structure, and electrical and thermal transport properties of quinary stannites $Cu_{2.2}Zn_{0.8}SnSe_{4-x}Te_x$ with $0.1 \leq x \leq 0.4$. We investigated alloying

of Se-based stannites with Te while maintaining a higher than stoichiometric Cu content since excess Cu has been shown to enhance the thermoelectric properties of these materials.[5,15]

RESULTS AND DISCUSSION

Powder X-ray diffraction (XRD) revealed single-phase specimens with the stannite crystal structure for each composition. The lattice parameters for this tetragonal structure were first estimated and then refined. The initial positional parameters for all the atoms in the structure were from data on $Cu_2ZnSnSe_4$.[18] For all specimens the space group $I\bar{4}2m$ (#121) was applied to refine the crystal structure. The excess Cu is located at the crystallographic 2*a* site along with Zn while Te and Se are on the crystallographic 8*i* site. Site occupancy refinements of each atom for each composition were carried out to check for any structural disorder. Zinc has a 98 % occupancy in $Cu_{2.2}Zn_{0.8}SnSe_{3.8}Te_{0.2}$, with the other sites fully occupied, while each atom for the other three compositions are fully occupied. The atomic coordinates, displacement parameters, and fractional parameters were refined with constraint first, and the final values obtained were with full least-square refinements. The observed and calculated XRD patterns and the difference profiles for each specimen are given in Figure 1. Detailed refinement results are shown in Table 1. Figure 2 shows the crystal structure of $Cu_{2.2}Zn_{0.8}SnSe_{4-x}Te_x$ based on our refinement results. Each metal atom is surrounded by four Se/Te atoms in a tetrahedral geometry. Each Se/Te atom is also tetrahedrally bounded by four metal atoms (two Cu1, one Zn/Cu2, and Sn). As expected the lattice parameters and bond distances increase with increasing Te content. Metal-Se/Te bond distances range from 2.43291(4) Å to 2.4449(3) Å for Cu1, 2.43582(4) Å to 2.4526(3) Å for Zn/Cu2, and 2.53537(4) Å to 2.5503(3) Å for Sn. As expected when alloying with Te, these bond distances are somewhat longer than the metal-Se bond distances in $Cu_2ZnSnSe_4$[18] and

$Cu_{2.2}Zn_{0.8}SnSe_4$.[15] The compositions obtained from our refinements are consistent with those obtained from elemental analyses. Figure 3 shows a scanning electron microscopy (SEM) image and energy dispersive X-ray analysis (EDX) elemental mapping images of the hot pressed $Cu_{2.2}Zn_{0.8}SnSe_{3.8}Te_{0.2}$ specimen as representative of our analyses. EDX analyses revealed that each element was uniformly distributed, corroborating our XRD results.

Figures 4(a) and 4(b) show temperature dependent ρ and S values, respectively, for all four specimens. The temperature dependence of ρ for $Cu_{2.2}Zn_{0.8}SnSe_{3.9}Te_{0.1}$, $Cu_{2.2}Zn_{0.8}SnSe_{3.7}Te_{0.3}$, and $Cu_{2.2}Zn_{0.8}SnSe_{3.6}Te_{0.4}$ is relatively flat up to 500 K and then increases slowly with increasing temperature. The ρ values for $Cu_{2.2}Zn_{0.8}SnSe_{3.8}Te_{0.2}$ decrease with increasing temperature up to 500 K and then increase slightly with increasing temperature. The different behavior for the $Cu_{2.2}Zn_{0.8}SnSe_{3.8}Te_{0.2}$ specimen below 500 K is presumably due to the Zn deficiency which may act as hole traps. The $Cu_{2.2}Zn_{0.8}SnSe_{3.8}Te_{0.2}$ specimen has a smaller hole concentration than that of the other specimens, from our Hall measurements described below. The increase in ρ above 500 K for all specimens may be due to structural-disorder inducing a reduction in carrier mobility.[19] UV / Vis diffuse spectroscopy measurements were carried out for all four specimens however the spectra did not show any absorption edge over the entire measurement range (2700 nm to 200 nm; 0.46 eV to 6.22eV). This indicated that these compounds possess band gaps below 0.46 eV. We therefore estimated the band gap of these compounds from the temperature dependent electrical conductivity data. The inset in Figure 4(a) shows a plot of ln(σ) vs 1/T for $Cu_{2.2}Zn_{0.8}SnSe_{3.7}Te_{0.3}$ as an example. The solid line in this figure is a fit to the highest temperature data using $\sigma = \sigma_o \, exp(-E_g / 2k_BT)$ where E_g is the band gap and k_B is the Boltzmann constant. The E_g values obtained in this way are 0.13 eV for $Cu_{2.2}Zn_{0.8}SnSe_{3.9}Te_{0.1}$, 0.23 eV for

$Cu_{2.2}Zn_{0.8}SnSe_{3.8}Te_{0.2}$, 0.23 eV for $Cu_{2.2}Zn_{0.8}SnSe_{3.7}Te_{0.3}$, and 0.29 eV for $Cu_{2.2}Zn_{0.8}SnSe_{3.6}Te_{0.4}$. Tellurium alloying results in narrower band-gaps in these materials as compared with $Cu_2ZnSnSe_4$ and Cu_2ZnSnS_4,[20,21] a property of interest in thermoelectric materials, and indicates that band-gap tuning is possible with Te substitution. All specimens exhibit positive *S* values, as expected for these *p*-type materials, with increasing *S* with temperature up to the maximum measured temperature. Consistent with the *S* data, Hall measurements indicated that holes are the majority carriers for all specimens, with room temperature carrier concentrations, *p*, of 1.2 x $10^{21}/cm^3$ for $Cu_{2.2}Zn_{0.8}SnSe_{3.9}Te_{0.1}$, 5.3 x $10^{20}/cm^3$ for $Cu_{2.2}Zn_{0.8}SnSe_{3.8}Te_{0.2}$, 6.2 x $10^{20}/cm^3$ for $Cu_{2.2}Zn_{0.8}SnSe_{3.7}Te_{0.3}$, and 6.6 x $10^{20}/cm^3$ for $Cu_{2.2}Zn_{0.8}SnSe_{3.6}Te_{0.4}$. The carrier mobility for each specimen was evaluated from ρ and Hall data at room temperature. The hole mobilities are very low and decrease with increasing Te contents (2.9 cm^2 / V·s for $Cu_{2.2}Zn_{0.8}SnSe_{3.9}Te_{0.1}$, 1.5 cm^2 / V·s for $Cu_{2.2}Zn_{0.8}SnSe_{3.8}Te_{0.2}$, 1.8 cm^2 / V·s for $Cu_{2.2}Zn_{0.8}SnSe_{3.7}Te_{0.3}$, and 1.7 cm^2 / V·s for $Cu_{2.2}Zn_{0.8}SnSe_{3.6}Te_{0.4}$.), however, the room temperature mobility for $Cu_{2.2}Zn_{0.8}SnSe_{3.8}Te_{0.2}$ is lower than that of the two higher Te content specimens. This is presumably due to the vacancies on the 2*a* site in this compound, as described above.

Assuming a single parabolic band model, *S* and *p* are given by[22]

$$S = \frac{k_B}{e}\left(\frac{(2+r)F_{1+r}(\eta)}{(1+r)F_r(\eta)} - \eta\right) \qquad (1)$$

and

$$p = \frac{4\pi(2m_e k_B T)^{3/2}}{h^3}\left(\frac{m^*}{m_e}\right)^{3/2} F_{1/2}(\eta) \qquad (2)$$

where r is the exponent of the energy dependence of the electron mean free path, η (= E_F / k_BT) is the reduced Fermi energy, E_F is the Fermi energy, F_r is the Fermi integral of order r,[23,24] m^* is the hole effective mass, m_e is the free electron mass, and h is the Planck constant. For scattering from lattice vibrations (acoustic phonons) $r = 0$ and for ionized impurity scattering $r = 2$. In our estimate of m^* we used the intermediate value $r = 1$. From our room temperature S and n values we obtain $m^* = 1.4\ m_e$ for $Cu_{2.2}Zn_{0.8}SnSe_{3.9}Te_{0.1}$, $m^* = 1.7\ m_e$ for $Cu_{2.2}Zn_{0.8}SnSe_{3.8}Te_{0.2}$, $m^* = 1.6\ m_e$ for $Cu_{2.2}Zn_{0.8}SnSe_{3.7}Te_{0.3}$, and $m^* = 1.5\ m_e$ for $Cu_{2.2}Zn_{0.8}SnSe_{3.6}Te_{0.4}$, values that are similar to that of other stannite compositions (1.2 m_e).[9]

The high temperature κ values are shown in Figure 5(a). The κ values decrease gradually with increasing temperature. The κ_L values (Figure 5(b)) were estimated using the Wiedemann-Franz relation $\kappa = \kappa_E + \kappa_L$, where $\kappa_E = L_0\sigma T$, σ is the electrical conductivity, $\sigma = 1/\rho$, and $L_0 = 2.0 \times 10^{-8}\ V^2/K^2$, the Lorenz number,[5,6] and indicate that κ_L is the dominant contribution in these specimens due to the relatively high ρ values for all specimens. The temperature dependence of κ_L is proportional to T^{-1} over the entire measurement range thus the contribution to κ by bipolar diffusion, κ_B, can be estimated from the available data at elevated temperatures (see inset in Figure 5(b)). Here κ_B is the difference between the fit line and κ_L at the highest temperatures. As shown in this figure the contribution of κ_B is very small at high temperatures with no significant "upturn" in the data at the highest temperatures. This is indicative of little or no bipolar contribution to κ in the measured temperature range for all specimens. This also agrees with the S data which shows no sign of a peak or deviation in slope at the higher temperatures that would be indicative of bipolar diffusion.

The *ZT* values for all specimens were calculated using the data in Figures 4 and 5 and are shown in Figure 6. The *ZT* values for all specimens increase rapidly with increasing temperature. The highest *ZT* value (0.56) was obtained at 700 K for $Cu_{2.2}Zn_{0.8}SnSe_{3.7}Te_{0.3}$ specimens. $Cu_{2.2}Zn_{0.8}SnSe_{3.8}Te_{0.2}$ also has a relatively high *ZT*, from a low κ_L and a high *S* due to the Zn deficiency, and may represent another avenue for thermoelectric properties enhancements in these materials.

EXPERIMENTAL

Synthesis. All compounds were prepared by direct reaction of high purity elements. Cu powder (99.9 %, Alfa Aesar), Zn shot (99.9999 %, Alfa Aesar), Sn powder (99.999 %, Alfa Aesar), Se powder (99.999 %, Alfa Aesar), and Te ingot (99.99+%, Strem) were loaded into silica ampoules in stoichiometric ratios $Cu_{2.2}Zn_{0.8}SnSe_{4-x}Te_x$ (where x = 0.1, 0.2, 0.3, and 0.4). The reaction ampoules were sealed in quartz tubes, heated to 973 K and subsequently held at this temperature for 4 days. The furnace was turned off and the reaction tubes were quenched to room temperature in air. The products were then ground into fine powders, cold pressed into pellets and annealed at 973 K for one week, with an additional grinding and annealing step performed in order to further promote homogeneity of the products. After appropriate annealing the products were ground into fine powders and sieved (325 mesh) inside a glovebox before loaded into graphite dies for hot pressing. Densification was accomplished by hot pressing at 673 K and 150 MPa for 3 hours under N_2 flow. The density of the hot-pressed pellets was determined by measurement of their dimensions and weight after polishing the surfaces of the pellets. These measurements indicated that high density polycrystalline specimens (> 96 % of theoretical density) were obtained.

Physical Characterization. XRD and electron probe analyses were used to examine the purity and chemical composition of the specimens. Powder XRD data were collected with a Bruker D8 Focus diffractometer in Bragg-Brentano geometry using Cu $K_{\alpha,\beta}$ radiation and a graphite monochromator, and examined by the Rietveld method using the GSAS suite of programs.[25,26] EDX of the hot-pressed pellets was accomplished with an Oxford INCA X-Sight 7582M equipped SEM (JEOL JSM-6390LV). The average atomic ratios were calculated from at least twelve data sets obtained from random positions of the hot pressed pellet for each specimen. Optical diffuse reflectance measurements were performed at room temperature using a JASCO V-670 UV-Vis double beam Spectrophotometer. The instrument is equipped with a 60 mm diameter integrating sphere. A fine powder for each specimen was prepared by grinding the polycrystalline specimen that was then compacted between two quartz slides. Reflectance data were collected in the wavelength range of 200 ~ 2700 nm.

High temperature S and ρ were measured on parallelepipeds (2mm x 2mm x 10mm), cut from the hot pressed pellets, with an ULVAC ZEM-3 system (experimental uncertainty of 5~8 % for S and ρ at elevated temperatures). High temperature κ values were determined using the equation $\kappa = D \cdot \alpha \cdot C_p$ where D is the measured density from geometry, α is the measured thermal diffusivity, and C_p is the specific heat. Thermal diffusivity measurements employed the laser flash method in a flowing He environment with a NETZSCH LFA 457 system. The uncertainty in the thermal diffusivity measurements were ~5 %. Heat capacity C_p ($\approx C_v$) was estimated with the Dulong-Petit limit ($C_v = 3nR$, where n is the number of atoms per formula unit and R is the ideal gas constant). At high temperature this may sometimes result in an underestimation of C_p, thus affecting κ, however it is a relatively good method for comparing the effect of doping and compositional changes since it eliminates the uncertainties associated with C_p measurements.[27]

The *S* and ρ measurements were performed perpendicular to the pressing axis, whereas the laser flash diffusivity measurements were carried out on the entire pellet parallel to the pressing axis. Room-temperature four-probe Hall measurements with 0.5 mm × 2 mm × 5 mm parallelepipeds were conducted at multiple positive and negative magnetic fields in order to eliminate voltage probe misalignment effects.

CONCLUSION

Dense polycrystalline Se-Te alloy Cu excess stannites, $Cu_{2.2}Zn_{0.8}SnSe_{4-x}Te_x$ (x = 0.1, 0.2, 0.3, 0.4), were prepared and their structural and high temperature transport properties were investigated for the first time. Rietveld refinement and elemental analyses confirm the composition of each specimen to be very close to that of their nominal compositions. The unit cell parameters and metal-chalcogen bond distances increase with increasing Te content. The estimated band gaps, from high temperature σ values, indicate that all specimens possess relatively narrow band gaps, between 0.13 ~ 0.29 eV, as compared to most other stannite compositions. Increasing *S* values and decreasing κ values with increasing temperature, without a peak for either *S* or κ, indicate that bipolar diffusion is negligible for those compositions. A *ZT* value of 0.56 was obtained at 700 K for $Cu_{2.2}Zn_{0.8}SnSe_{3.7}Te_{0.3}$, the specimen for which κ_L was lowest, and is higher than that of $Cu_2ZnSnSe_4$ (~ 0.2 at 700 K) and $Cu_2ZnGeSe_{4-x}S_x$ (~ 0.2 at 650 K).[5,14]

ACKNOWLEDGEMENTS

The work was supported by the National Science Foundation Grant No. DMR-1400957. H.W. would like to thank the support of the assistant secretary for Energy Efficiency and Renewable

Energy of the Department of Energy and the Propulsion Materials program under the Vehicle Technologies program. Oak Ridge National Laboratory is managed by UT-Battelle LLC under contract DE-AC05000OR22725. The work in Dr. Tritt's laboratory acknowledges, in a small part, the support of a KAUST Faculty Initiated Collaboration grant and also internal funding from Clemson University.

REFERENCES

1. T. M. Tritt, *Ann*. *Rev*. *Mater*. *Res*., 2011, **41**, 433-448.

2. F. J. DiSalvo, *Science*, 1999, **285**, 703-706.

3. G. S. Nolas, J. W. Sharp and H. J. Goldsmid, *Thermoelectrics: Basics Principles and New Materials Developments*; Springer-Verlag: 2001.

4. G. D. Mahan, *Solid State Phys*., 1998, **51**, 81-157.

5. M. L. Liu, F. Q. Huang, L. D. Chen and I. W. Chen, *Appl*. *Phys*. *Lett*., 2009, **94**, 202103.

6. M. L. Liu, I. W. Chen, F. Q. Huang and L. D. Chen, *Adv*. *Mater*., 2009, **21**, 3808-3812.

7. M. Ibáñez, D. Cadavid, R. Zamani, N. García-Castelló, V. Izquierdo-Roca, W. Li, A. Fairbrother, J. D. Prades, A. Shavel, J. Arbiol, A. Pérez-Rodríguez, J. R. Morante and A. Cabot, *Chem*. *Mater*., 2012, **24**, 562-570.

8. M. Ibáñez, R. Zamani, A. LaLonde, D. Cadavid, W. Li, A. Shavel, J. Arbiol, J. R. Morante, S. Gorsse, G. J. Snyder and A. Cabot, *J*. *Am*. *Chem*. *Soc*., 2012, **134**, 4060-4063.

9. W. G. Zeier, A. LaLonde, Z. M. Gibbs, C. P. Heinrich, M. Panthöfer, G. J. Snyder and W. Tremel, *J*. *Am*. *Chem*. *Soc*., 2012, **134**, 7147-7154.

10. X. Y. Shi, F. Q. Huang, M. L. Liu and L. D. Chen, *Appl*. *Phys*. *Lett*., 2009, **94**, 122103.

11. Ch. Raju, M. Falmbigl, P. Rogl, X. Yan, E. Bauer, J. Horky, M. Zehetbauer and R. C. Mallik, *AIP Adv*., 2013, **3**, 032106.

12. W. G. Zeier, Y. Pei, G. Pomrehn, T. Day, N. Heinz, C. P. Heinrich, G. J. Snyder and W. Tremel, *J*. *Am*. *Chem*. *Soc*., 2013, **135**, 726-732.

13. Y. Dong, H. Wang and G. S. Nolas, *Inorg*. *Chem*., 2013, **52**, 14364-14367.

14. C. P. Heinrich, T. W. Day, W. G. Zeier, G. J. Snyder and W. Tremel, *J*. *Am*. *Chem*. *Soc*., 2014, **136**, 442-448.

15. Y. Dong, H. Wang and G. S. Nolas, *Phys*. *Status Solidi RRL*, 2014, **8**, 61-64.

16. J. Navrátil, V. Kucek, T. Plecháček, E. Černošková, F. Laufek, Č. Drašar and P. Kmotek, *J. Electron*. *Mater*., 2014, **43**, 3719-3725.

17. R. Chetty, J. Dadda, J. de Boor, E. Müller and R. C. Mallik, *Intermetallics*, 2015, **57**, 156-162.

18. I. D. Olekseyuk, L. D. Gulay, I. V. Dydchak, L. V. Piskach, O. V. Parasyuk and O. V. Marchuk, *J*. *Alloys Compd*., 2002, **340**, 141-145.

19. H. Wang, A. D. Lalonde, Y. Pei and G. J. Snyder, *Adv*. *Funct*. *Mater*., 2013, **23**, 1586-1596.

20. R. Adhi Wibowo, E. S. Lee, B. Munir and K. H. Kim, *Phys*. *Status Solidi* A, 2007, **204**, 3373.

21. F. Jiang, H. Shen and W. Wang, *J*. *Electron*. *Mater*., 2012, **41**, 2204.

22. G. A. Slack and M. A. Hussain, *J*. *Appl*. *Phys*., 1991, **70**, 2694-2718.

23. P. Rhodes, *Proc*. *R*. *Soc*. *London A*, 1950, **204**, 396-405.

24. J. McDougall and E. C. Stoner, *Philos*. *Trans*. *R*. *Soc*. *London A*, 1938, **237**, 67-104.

25. A. C. Larson and R. B. Von Dreele, *General Structure Analysis System*, Report LAUR 86-748, Los Alamos National Laboratory, 2004.

26. B. H. Toby, *J*. *Appl*. *Cryst*., 2001, **34**, 210-221.

27. H. Wang, W. D. Porter, H. Bottner, J. Kronig, L. Chen, S. Bai, T. M. Tritt, A. Mayolet, J. Senawiratne, C. Smith, F. Harris, P. Gillbert, J. Sharp, J. Lo, H. Kleinke and L. Kiss, *J*. *Electron*. *Mater*., 2013, **42**, 1073-1084.

Table 1. Rietveld refinement[a)] results for $Cu_{2.2}Zn_{0.8}SnSe_{4-x}Te_x$.

Composition	$Cu_{2.2}Zn_{0.8}SnSe_{3.9}Te_{0.1}$	$Cu_{2.2}Zn_{0.8}SnSe_{3.8}Te_{0.2}$	$Cu_{2.2}Zn_{0.8}SnSe_{3.7}Te_{0.3}$	$Cu_{2.2}Zn_{0.8}SnSe_{3.6}Te_{0.4}$
EDX	$Cu_{2.2}Zn_{0.8}Sn_{0.9}Se_{3.9}Te_{0.1}$	$Cu_{2.2}Zn_{0.8}Sn_1Se_{3.8}Te_{0.2}$	$Cu_{2.2}Zn_{0.8}Sn_{1.1}Se_{3.6}Te_{0.3}$	$Cu_{2.2}Zn_{0.8}Sn_{1.1}Se_{3.6}Te_{0.4}$
Space group, Z	$I\bar{4}2m$ (#121), 2			
a, Å	5.6835 (1)	5.6970 (2)	5.7085 (3)	5.7151 (8)
c, Å	11.3311 (4)	11.3608 (7)	11.3823 (8)	11.397 (2)
V, Å^3	366.02 (2)	368.73 (3)	370.91 (6)	372.3 (1)
Radiation	Graphite monochromated Cu Kα (1.54056 Å)			
$D_{calc.}$, g/cm^3	5.720	5.724	5.746	5.750
variables	11	9	18	13
wR_p, R_p	0.0598, 0.0434	0.0804, 0.0572	0.0655, 0.0487	0.0708, 0.0507
$R(F^2)$	0.1080	0.1249	0.1599	0.1130
Cu1-Se/Te, Å	2.43291 (4)	2.43919 (7)	2.4427 (1)	2.4449 (3)
Zn/Cu2-Se/Te, Å	2.43582 (4)	2.43955 (8)	2.4490 (1)	2.4526 (3)
Sn-Se/Te, Å	2.53537 (4)	2.54345 (8)	2.5462 (1)	2.5503 (3)
Se/Te, x and z	0.24234, 0.12908	0.24202, 0.12904	0.24255, 0.12923	0.24251, 0.12934

[a)]Atomic positions: Cu1, 4*d* (0,0.5,0.25); Zn/Cu2, 2*a* (0,0,0); Sn, 2*b* (0,0,0.5); Se/Te, 8*i* (x,x,z)

Figure Captions

Figure 1. Powder XRD data for (a) $Cu_{2.2}Zn_{0.8}SnSe_{3.9}Te_{0.1}$, (b) $Cu_{2.2}Zn_{0.8}SnSe_{3.8}Te_{0.2}$, (c) $Cu_{2.2}Zn_{0.8}SnSe_{3.7}Te_{0.3}$, and (d) $Cu_{2.2}Zn_{0.8}SnSe_{3.6}Te_{0.4}$ including profile fit, profile difference, profile residuals, and Bragg positions (purple ticks) from Rietveld refinement.

Figure 2. Unit cell representation of $Cu_{2.2}Zn_{0.8}SnSe_{4-x}Te_x$. The Cu1 atoms are represented by red circles at the 4*d* crystallographic site, the Zn/Cu2 atoms are represented by blue/red circles at the 2*a* crystallographic site, the Sn atoms are represented by gray circles at the 2*b* crystallographic site, and the Se/Te atoms are represented by yellow/black circles at 8*i* crystallographic site.

Figure 3. (b) SEM and EDX elemental mapping images of hot-pressed $Cu_{2.2}Zn_{0.8}SnSe_{3.8}Te_{0.2}$.

Figure 4. Temperature dependent (a) ρ and (b) S data for $Cu_{2.2}Zn_{0.8}SnSe_{3.9}Te_{0.1}$ (▽), $Cu_{2.2}Zn_{0.8}SnSe_{3.8}Te_{0.2}$ (□),$Cu_{2.2}Zn_{0.8}SnSe_{3.7}Te_{0.3}$ (△), and $Cu_{2.2}Zn_{0.8}SnSe_{3.6}Te_{0.4}$ (○). The inset in (a) corresponds to the ln(σ) versus T^{-1} for $Cu_{2.2}Zn_{0.8}SnSe_{3.7}Te_{0.3}$ and the solid line is a fit of the form $\sigma = \sigma_0 \exp(-E_g / 2k_BT)$ to the highest-temperature data.

Figure 5. Temperature dependent (a) κ and (b) κ_L for $Cu_{2.2}Zn_{0.8}SnSe_{4-x}Te_x$. The inset in (b) illustrates our estimation of κ_B for $Cu_{2.2}Zn_{0.8}SnSe_{3.9}Te_{0.1}$ as an example. The solid line illustrates the T^{-1} dependence between 300 and 650K. The symbols corresponding to each specimen are as defined in Figure 4.

Figure 6. The dimensionless figure of merit, *ZT*, as a function of temperature for $Cu_{2.2}Zn_{0.8}SnSe_{4-x}Te_x$. The symbols corresponding to each specimen are as defined in Figure 4.

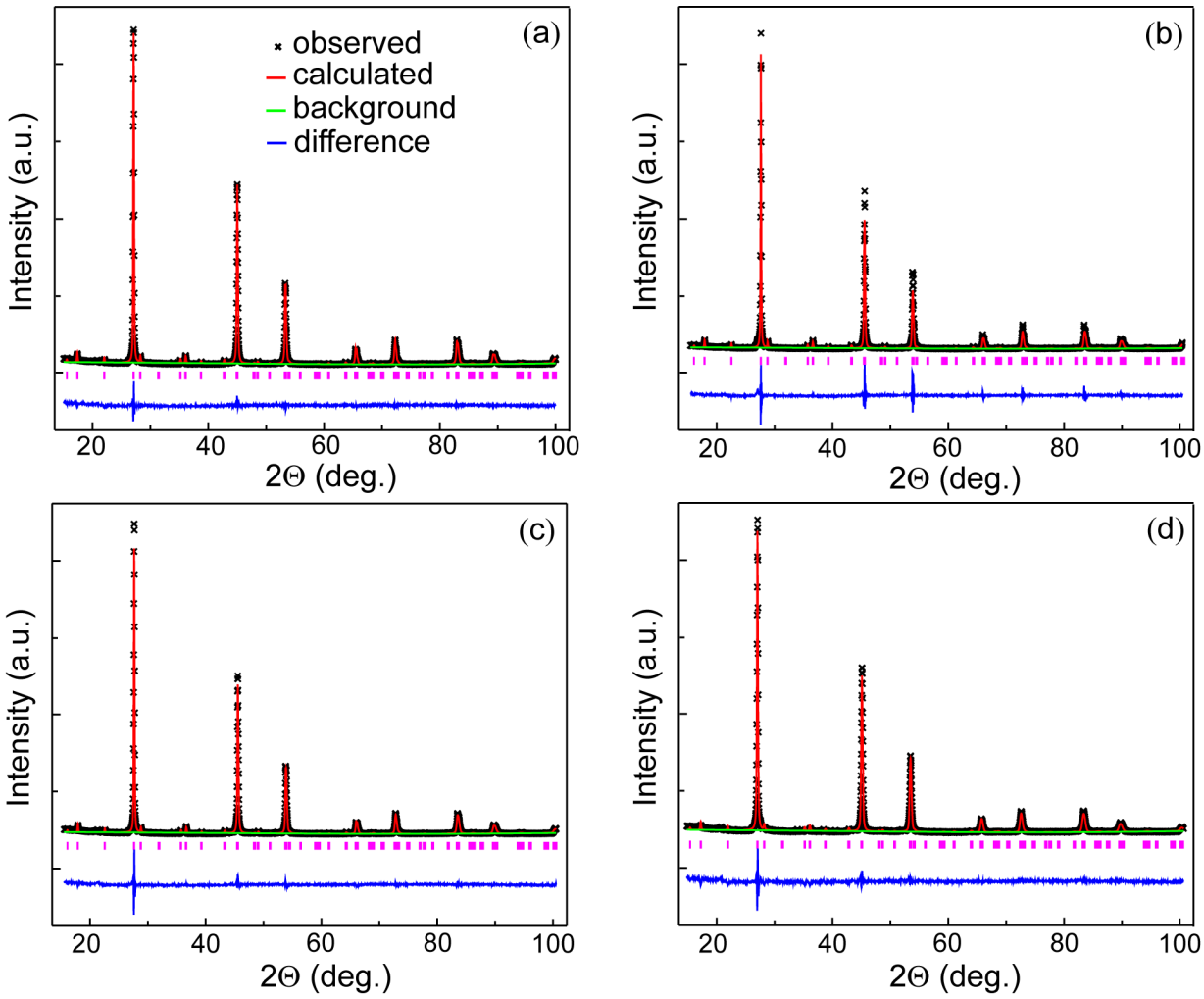

Figure 1.

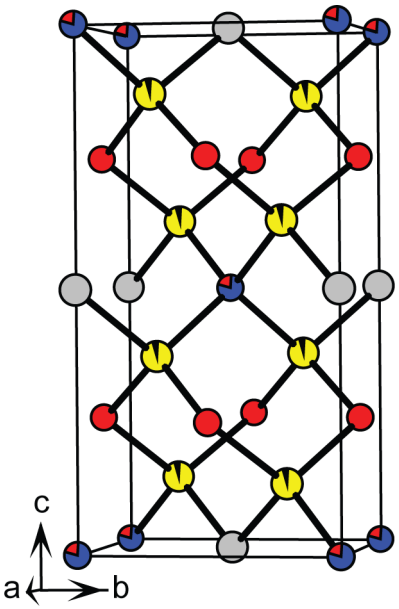

Figure 2.

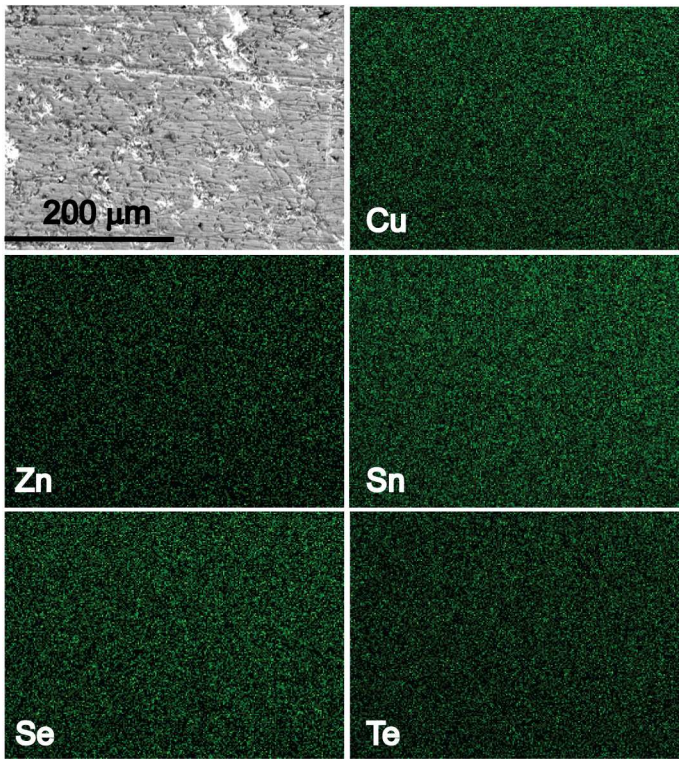

Figure 3.

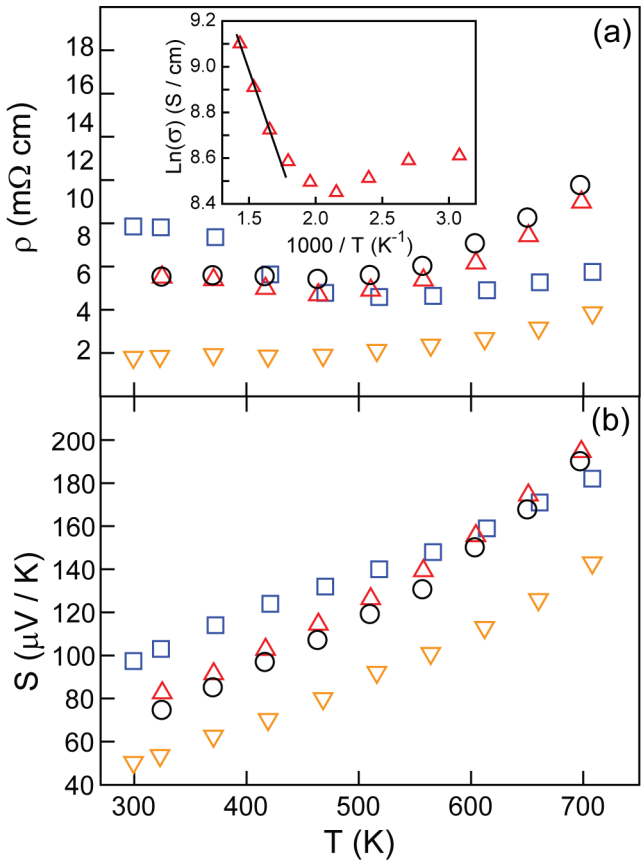

Figure 4.

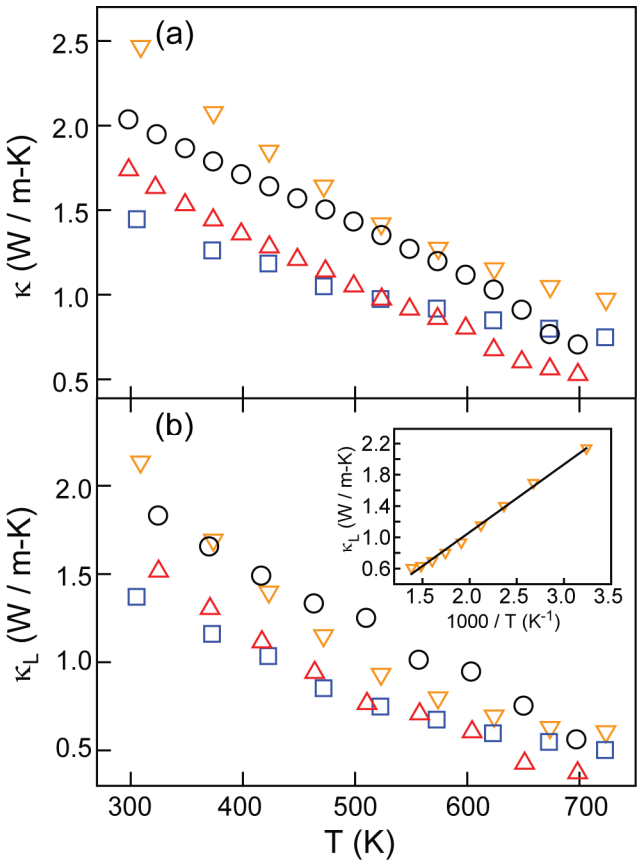

Figure 5.

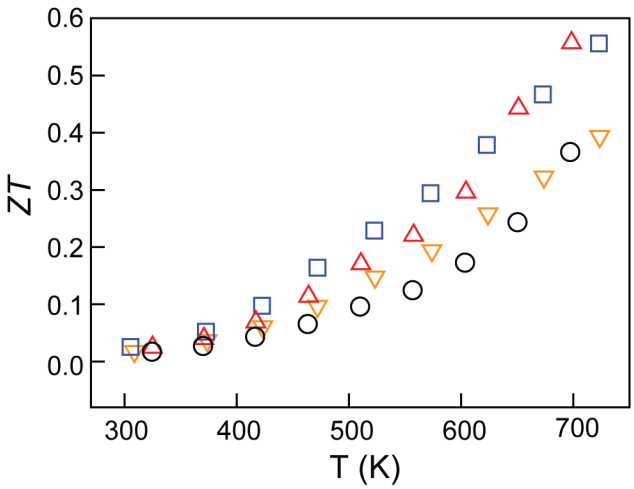

Figure 6.